DAWSON, B. (1967). *Proc. Roy. Soc.* A**298**, 255–263.
FEDOROV, F. I. (1968). *Theory of Elastic Waves in Crystals*. New York: Plenum Press.
HAMILTON, W. C. (1965). *Acta Cryst.* **18**, 502–510.
JAMES, R. W. & BRINDLEY, G. W. (1928). *Proc. Roy. Soc.* A**121**, 155–171.
JAYALAKSHMI, K. & VISWAMITRA, M. A. (1970). *Phys. Lett.* **32A**, 83–84.
KOESTER, L. & KNOPF, K. (1972). *Z. Naturforsch.* **27A**, 901–905.
KOESTER, L. & NISTLER, W. (1971). *Phys. Rev. Lett.* **27**, 956–958.
MERISALO, M. & INKINEN, O. (1968). Private Communication, quoted by Patomaki & Linkoaho (1969).
NILSSON, N. (1957). *Ark. Fys.* **12**, 247–257.
PATOMAKI, L. K. & LINKOAHO, M. V. (1969). *Acta Cryst.* A**25**, 304–305.
REID, J. S. & SMITH, T. (1970). *J. Phys. Chem. Solids*, **31**, 2689–2697.
SOLT, G., BUTT, N. M. & O'CONNOR (1973). *Acta Cryst.* A**29**, 228–231.
TAYLOR, R. I. & WILLIS, B. T. M. (1973). To be published.
WASASTJERNA, J. A. (1946). *Soc. Sci. Fenn. Commun. Phys. Math.* **13**, 1–24.
WILLIS, B. T. M. (1969). *Acta Cryst.* A**25**, 277–300.
WILSON, S. A. & COOPER, M. J. (1973). *Acta Cryst.* A**29**, 90–91.
ZACHARIASEN, W. H. (1967). *Acta Cryst.* **23**, 558–564.

Acta Cryst. (1973). A**29**, 520

Electron Diffraction Study of Short-Range-Order Diffuse Scattering from Disordered Cu–Pd and Cu–Pt Alloys

BY KENICHI OHSHIMA AND DENJIRO WATANABE
Department of Physics, Tohoku University, Sendai, Japan

(*Received* 4 *November* 1972; *accepted* 31 *March* 1973)

The short-range-order diffuse scattering from disordered Cu–Pd and Cu–Pt alloys has been studied by electron diffraction using thin foils prepared from bulk specimens. Twofold and fourfold splittings of diffuse scattering are observed at 100, 110 and equivalent positions in the composition ranges from about 13 to 60 at.% Pd in the Cu–Pd system and up to about 45 at.% Pt in the Cu–Pt system. The separation of the split maxima increases with Pd or Pt content. A close investigation has revealed that the split maxima correspond to the intersections of slightly curved diffuse streaks around the 100 and 110 positions. These results can be interpreted well using the Fermi-surface-imaging theory proposed by Krivoglaz, indicating that the interaction potential in these alloys mainly originates from conduction electrons, and that the diffuse scattering reflects the form of the Fermi surface, *i.e.* the flatness normal to the ⟨110⟩ directions.

1. Introduction

The short-range order in binary alloys can be studied by observing the distribution of diffuse scattering, and the short-range-order parameters representing the pair correlations of atoms are available from the quantitative intensity measurements on single crystals (Cowley, 1950; Clapp & Moss, 1966, 1968; Moss & Clapp, 1968; Wilkins, 1970). However, until recently the electron diffraction method was not considered to be suitable for this purpose, compared with the X-ray and neutron diffraction methods mainly because of the difficulty in quantitative intensity measurement in electron diffraction. Moreover, it was known that the distributions of diffuse scattering observed by electron diffraction for some alloys were different from those observed with X-rays. For example, for disordered Cu_3Au, CuAu and $CuAu_3$ alloys a cross-like distribution consisting of four diffuse spots was observed in electron diffraction (Raether, 1952; Marcinkowski & Zwell, 1963; Sato, Watanabe & Ogawa, 1962; Watanabe & Fisher, 1965), whereas a disk-like or nearly spherical or egg-shaped distribution without fine structure was concluded from X-ray diffractometer observations (Cowley, 1950; Roberts, 1954; Batterman, 1957). For these reasons, little attention had unduly been paid to the results of electron diffraction studies. However, the disagreements were removed recently by Moss (1966). He observed a cross-like distribution from disordered Cu_3Au in X-ray diffraction photographs also, in conformity with the electron diffraction observations.

The importance of the electron diffraction observation has recently increased significantly, since it was pointed out by Krivoglaz (1969) and Moss (1969) that the form of the Fermi surface of a disordered alloy is reflected in the distribution of short-range-order diffuse scattering through anomalies which are similar to those predicted by Kohn for phonon scattering and are due to the pair-interaction potential caused by conduction electrons in the alloy. This correlation between the diffuse-scattering intensity distribution and the Fermi

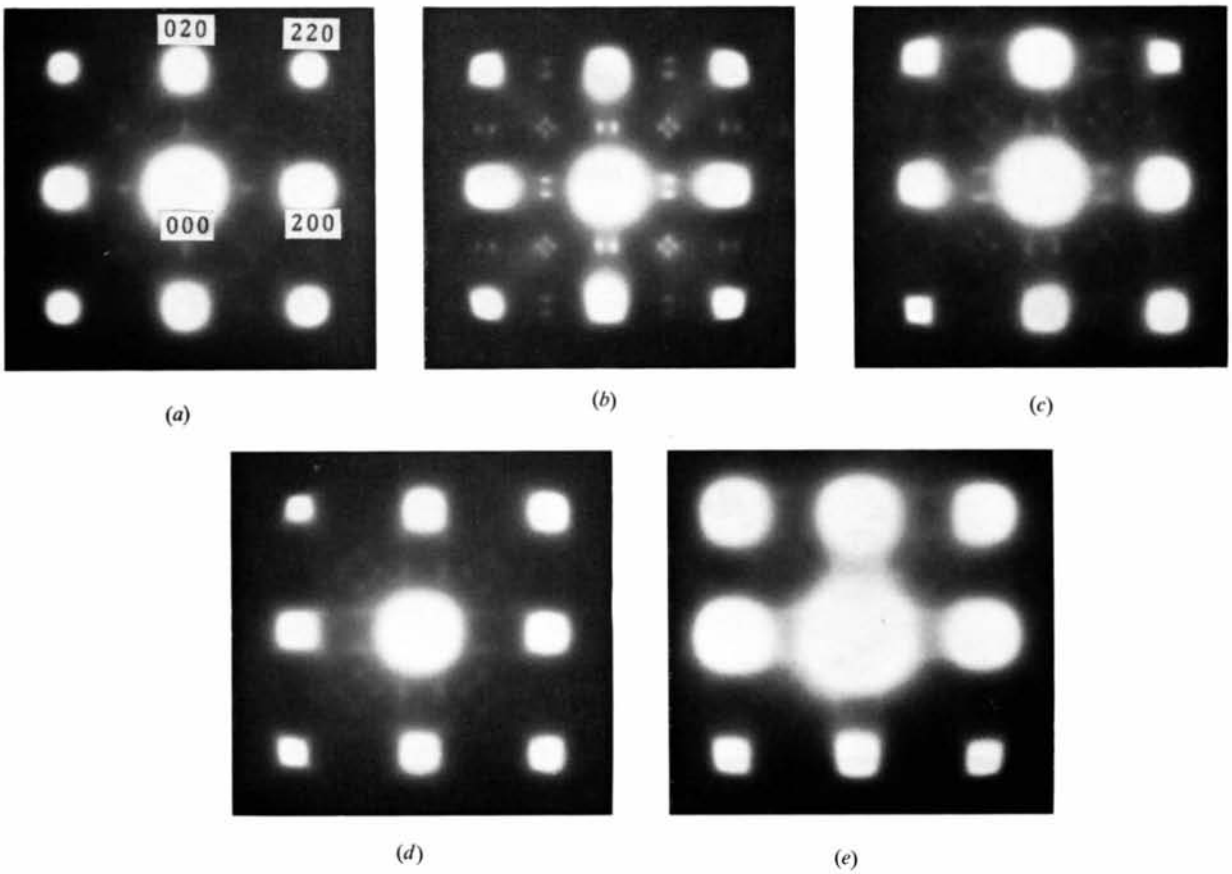

Fig. 1. Electron-diffraction patterns of disordered Cu–Pd alloys. Incident beam is parallel to [001] of the fundamental lattice. (*a*) 12·6 at.% Pd, (*b*) 25·0 at.% Pd, (*c*) 33·2 at.% Pd, (*d*) 41·0 at.% Pd and (*e*) 48·4 at.% Pd. Indices refer to the fundamental lattice.

[*To face p.* 520

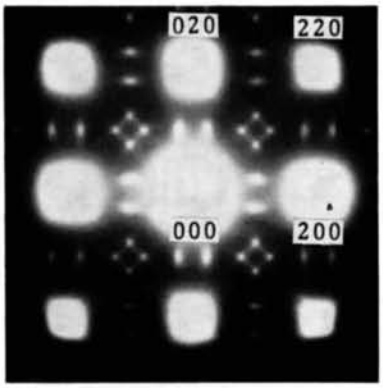

Fig. 3. Diffraction pattern of Cu–33·2 at. % Pd alloy quenched from 1000 °C. [001] incidence.

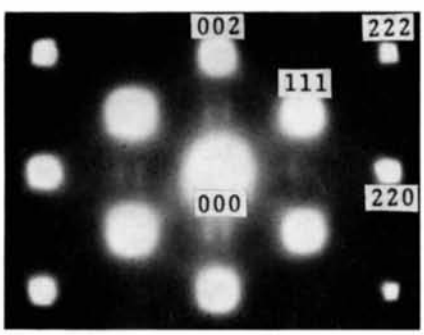

(*a*)

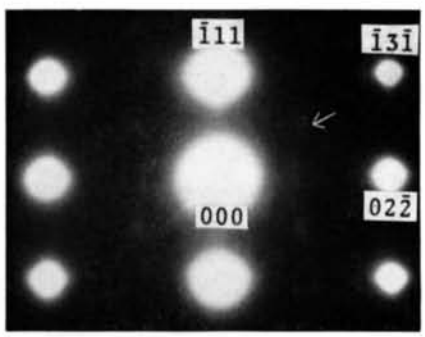

(*b*)

Fig. 4. Diffraction patterns of Cu–33·2 at. % Pd alloy quenched from 600 °C. (*a*) [1$\bar{1}$0] incidence, (*b*) [211] incidence.

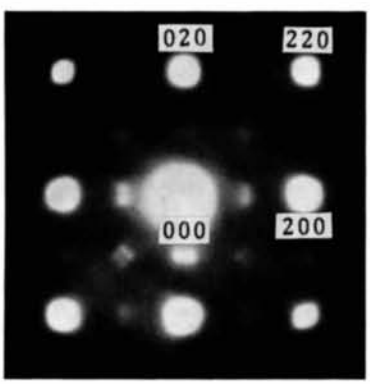

(*a*)

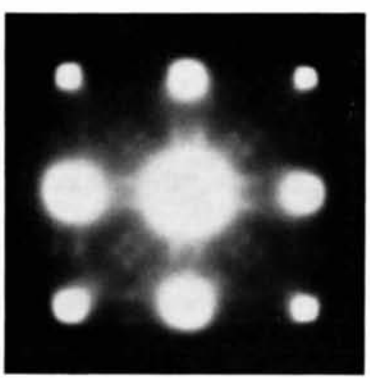

(*b*)

Fig. 5. Diffraction patterns of disordered Cu–Pt alloys. (*a*) 24·4 at. % Pt and (*b*) 35·0 at. % Pt. [001] incidence.

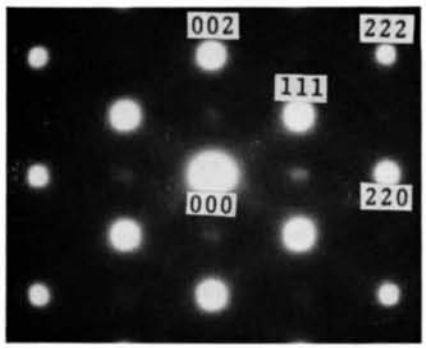

(*a*)

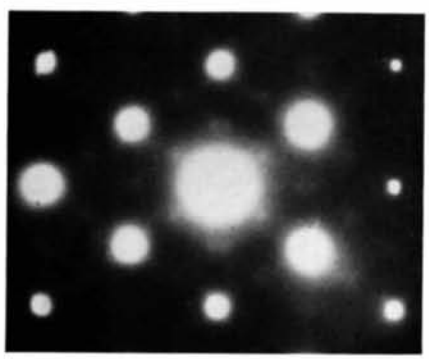

(*b*)

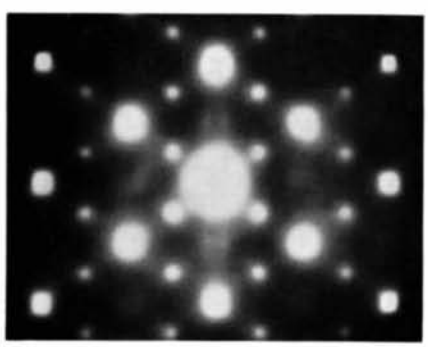

(*c*)

Fig. 6. Diffraction patterns of disordered Cu–Pt alloys. (*a*) 24·4 at. % Pt, (*b*) 29·8 at. % Pt and (*c*) 35·0 at. % Pt. Quenching temperatures are 680, 540 and 700 °C respectively. [1$\bar{1}$0] incidence.

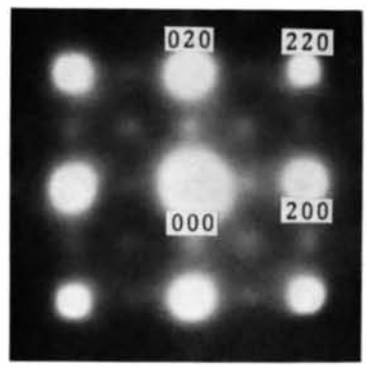

(*a*)

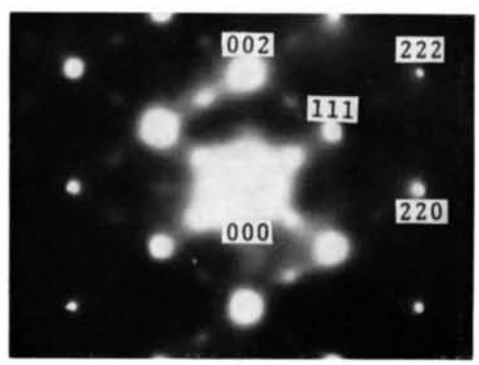

(*b*)

Fig. 7. Diffraction patterns of Cu–75·8 at. % Pt alloy quenched from 800 °C. (*a*) [001] incidence, (*b*) [1$\bar{1}$0] incidence.

surface may be observed in principle by any one of the X-ray, neutron and electron diffraction methods provided suitable single-crystal specimens are available. The electron diffraction method, however, is most advantageous because of the much greater ease in obtaining and interpreting single-crystal patterns.

In the present work the diffuse scattering from disordered Cu–Pd and Cu–Pt alloys is investigated in some detail by the electron diffraction method, using thin foils prepared from bulk specimens, with special reference to the composition dependence of the diffuse-scattering distribution. Whether the Fermi-surface-imaging idea proposed by Krivoglaz (1969) is applicable to these alloy systems was also studied.

It is well known that both the Cu–Pd and Cu–Pt alloy systems form continuous series of solid solutions with face-centred cubic structures at elevated temperatures (Hansen & Anderko, 1958). Below the composition-dependent critical temperatures, T_c, various types of superlattice structure are formed. In the Cu–Pd system, the alloys with compositions of 18 to 28 at. % Pd (α''-phase alloys) have periodic one-dimensional or two-dimensional anti-phase domain structures in the ordered state, depending on composition and temperature, of which the fundamental cell consists of a face-centred tetragonal atomic arrangement of the ordered Cu_3Au type. The alloys with Pd less than 18 at. % (α'-phase alloys) have the ordered Cu_3Au ($L1_2$) type structure with cubic symmetry (Watanabe & Ogawa, 1956; Hirabayashi & Ogawa, 1957; Michikami, Iwasaki & Ogawa, 1971). The β phase, found between 36 and 46 at. % Pd, has the CsCl ($B2$) type structure.

In the Cu–Pt system, the existence of three kinds of ordered phase, Cu_3Pt, CuPt and $CuPt_3$, has been established. In the alloys with Pt more than about 24 at. % of the Cu_3Pt phase region, a periodic one-dimensional anti-phase domain structure based on a face-centred tetragonal cell with an atomic arrangement of the ordered Cu_3Au type appears in the limited temperature range immediately below the critical ordering temperature T_c, although the $L1_2$ type structure is stable at lower temperatures (Schubert, Kiefer, Wilkens & Haufler, 1955; Ogawa, Iwasaki & Terada, 1973). The alloys in the Cu_3Pt region with Pt less than about 24 at. % have the $L1_2$-type structure in the whole temperature range below T_c. The CuPt phase has a rhombohedral superstructure of the $L1_1$ type consisting of alternating (111) planes of Cu and Pt atoms (Johansson & Linde, 1927; Schneider & Esch, 1944). In the $CuPt_3$ phase region, the existence of three different superlattice structures has recently been established, *i.e.*, the rhombohedral, orthorhombic and cubic phases, each depending on composition and temperature (Miida & Watanabe, 1973).

The high-temperature state of Cu_3Pd alloys above T_c has been studied by one of the present authors (Watanabe, 1959) on evaporated and oriented thin films, using a high-temperature electron-diffraction camera, and it was reported that the twofold and fourfold splittings of the diffuse scattering appear about 100, 110 and equivalent positions in reciprocal space, with the separation of the split maxima depending on the Pd content. This splitting was interpreted by considering the existence of micro anti-phase domains above T_c. X-ray studies of the short-range order in the Cu–Pt alloys have been made by Walker (1952) on a CuPt alloy and by Kaplow (1958) on the alloys with compositions ranging from 4 to 43 at. % Pt, and the short-range-order parameters were determined. However, the detailed distribution of the diffuse-scattering intensities in reciprocal space was not given, because powder samples were used in their studies.

The present experiment reveals that the splitting of the diffuse scattering appears in the compositions ranging from about 13 to 60 at. % Pd in the Cu–Pd system and up to about 45 at. % Pt in the Cu–Pt system, and the separation of the split maxima increases monotonically with increasing Pd or Pt content. The results are discussed in relation to the Fermi-surface-imaging theory.

2. Experimental

Bulk specimens were prepared within an atmosphere of purified argon in a plasma-jet arc furnace. The materials used were 99·999 % Cu, 99·9 % Pd and 99·9 % Pt. The specimens were homogenized by vacuum annealing for 5 days at 1000 °C, then rolled into thin sheets of 0·1–0·2 mm thick, heated again at 1000 °C to remove the strain and finally annealed at various temperatures above T_c.

Lattice parameters of the quenched specimens which are in the disordered state were measured with an X-ray Debye–Scherrer camera 114·6 mm in diameter with Cu $K\alpha$ radiation, using a Straumanis arrangement. Specimen compositions were determined with the accuracy of $\pm 0{\cdot}4$ at. % by referring to the lattice-parameter *vs.* composition relation (Pearson, 1958).

Thin foils suitable for transmission electron microscopy were obtained by electropolishing of the heat-treated sheets. The electrolytes consisted of 20 % nitric acid and 80 % methanol for Cu–Pd alloys (jet electropolishing) and 20 % nitric acid and 80 % hydrochloric acid for Cu–Pt alloys. A JEM-7A electron microscope equipped with a specimen-tilting device was operated at 100 kV, and electron-diffraction patterns for different orientations were obtained. Most of the patterns were taken from the specimens quenched from temperatures higher than T_c. The specimens were vacuum-sealed in silica tubes and the quenching was performed by dropping the tubes into iced water. Strictly speaking, a quenched specimen does not correspond to the equilibrium state appropriate to a specified temperature. However, as no superlattice spots appeared, it was assumed that the diffraction patterns obtained from a quenched specimen are those corresponding to the state of disorder at temperatures above T_c. A direct confir-

mation of this assumption was made for some specimens by observing diffraction patterns at high temperatures.

3. Results

3.1. Cu–Pd *system*

Specimens of various compositions ranging from 7·6 to 75·2 at.% Pd were prepared and the electron-diffraction patterns were examined for the quenched state. The diffuse scattering due to the short-range order was observed in the specimens containing 12·6 to 60·6 at.% Pd. Typical diffraction patterns for the specimens containing 12·6, 25·0, 33·2, 41·0 and 48·4 at.% Pd with the incident beam parallel to the [001] axis are shown in Fig. 1(*a*)–(*e*). The quenching temperatures were 600, 500, 600, 620 and 540°C, respectively. The alloys were isothermally heat-treated at these temperatures for 6–13 days prior to quenching. These patterns show that the intensity of diffuse scattering depends on the specimen composition. The intensity increases at first with increasing Pd content, and after attaining the maximum at about 25–33 at.% Pd, it decreases with a further increase of Pd content. The short-range-order diffuse scattering was not detected in the specimens with 7·6 and 75·2 at.% Pd.

Not only the intensity but also the intensity distribution changes remarkably with the Pd concentration. Except for the 12·6 at.% Pd alloy, twofold and fourfold splittings of the diffuse scattering are seen at 100, 110 and equivalent positions, with separations which are strongly composition dependent. The separation m as defined in Fig. 2 was measured in terms of the distance between the 000 and 200 fundamental spots. The distance m shows a monotonic increase with Pd concentration, as seen in Table 1.

Another important feature is the peculiar shape of the diffuse scattering at 110 and its equivalent positions, which consists of four weak and diffuse streaks with a slight curvature, as seen in Fig. 1(*b*)–(*e*). The positions of fourfold split maxima correspond to the intersections of these diffuse streaks, as schematically illustrated in Fig. 2. The streaks are more clearly seen for the specimen quenched from higher temperatures. Fig. 3 shows such an example of the 33·2 at.% Pd alloy quenched from 1000°C.

In order to confirm that the quenched specimens have the same short-range-ordered structures as those at temperatures above T_c, the diffraction patterns from the 25·0 and 29·4 at.% Pd alloys at high temperatures, about 500°C ($> T_c$), were also observed by the use of a hot stage of the electron microscope. The distributions of the short-range-order diffuse scattering from these specimens were the same as those obtained from quenched specimens but with stronger background intensities, and the values of m coincided well with those obtained for quenched specimens within the experimental error, as shown in Table 1. It should also be mentioned that a previous electron diffraction study performed by one of the present authors (Watanabe, 1959) on high-temperature specimens of the 13, 25 and 28 at.% Pd alloys gave essentially the same results as in the present study. The measured values of m in the previous results are also reproduced in Table 1 for comparison. It is, therefore, likely that the quenched specimens retain the short-range-ordered state existing at temperatures above T_c.

It is to be noted, however, that the diffuse-scattering intensity increases remarkably with increase in quenching temperature, as seen by comparing Fig. 1(*c*) with Fig. 3, whereby the separation m of split maxima does not change within the experimental error. This behaviour is

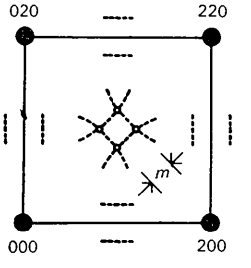

Fig. 2. Illustration of diffuse scattering in Fig. 1.

Table 1. *Values of separation m measured in terms of the distance between* 000 *and* 200 *spots for* Cu–Pd *alloys*

Composition x in $Cu_{1-x}Pd_x$	Quenching temperature (°C)	m measured at quenched state	m measured at 500°C	m measured at temperature by Watanabe (1959)
0·126	540	0		
0·130				0
0·184	600	0·048 ± 0·005		
0·228	520	0·086 ± 0·005		
0·250	500	0·095 ± 0·005	0·10 ± 0·01	0·091
0·280				0·114
0·294	500	0·137 ± 0·005	0·14 ± 0·01	
0·332	600	0·169 ± 0·005		
0·356	620	0·182 ± 0·005		
0·410	620	0·226 ± 0·008		
0·436	600	0·241 ± 0·008		
0·484	540	0·268 ± 0·008		
0·544	480	0·31 ± 0·01		
0·606	480	0·33 ± 0·02		

understood if in the course of quenching the atomic ordering is accelerated by vacancies in thermal equilibrium at high temperatures, so that the diffuse scattering intensity is enhanced with increasing quenching temperature, as the number of vacancies in thermal equilibrium increases with temperature.

In the present experiment, the diffraction patterns for the incident beams parallel to [001], [110], [111], [211] *etc.* were taken from quenched specimens and the diffuse-intensity distributions in reciprocal space were searched for. Fig. 4 (*a*) and (*b*) shows the diffraction patterns with [1$\bar{1}$0] and [211] incidence from the 33·2 at.% Pd alloy.

3.2. Cu–Pt *system*

Specimens of various compositions containing 5·6 to 75·8 at.% Pt were prepared and quenched from temperatures above the composition-dependent critical temperatures T_c. It was not easy to prepare thin foils of these alloys by the electropolishing technique particularly for the copper-rich range, and thin foils without an oxide film could not be obtained for alloys containing less than about 20 at.% Pt. Therefore, electron-diffraction patterns were taken only for the alloys with more than 24·4 at.% Pt.

Fig. 5 (*a*) and (*b*) shows typical diffraction patterns with [001] incidence for copper-rich specimens with 24·4 and 35·0 at.% Pt quenched from 680 and 700 °C after isothermal treatment for 12 and 5 days respectively. Twofold and fourfold splittings of the diffuse scattering at 100, 110 and equivalent positions bear a close resemblance to those in the case of the Cu–Pd system. The intensity decreases and the separation m increases with increasing Pt concentration, and the split maxima are visible up to 44·6 at.% Pt. The measured values of m are given in Table 2.

In the patterns of other orientations, on the other hand, the aspect of diffuse-scattering intensity distributions for the Cu–Pt system is quite different from that for the Cu–Pd system. For the Cu–Pt system additional diffuse intensities are observed at $\frac{111}{222}$ and equivalent positions. Although the intensity is very weak for the 24·4 at.% Pt alloy, it increases with the Pt concentration contrary to the intensity variation of the split maxima, as seen in Fig. 6(*a*)–(*c*) which are the diffraction patterns for [1$\bar{1}$0] incidence taken for the 24·4, 29·8 and 35·0 at.% Pt alloys respectively. The diffuse peaks at the $\frac{111}{222}$ positions are much weaker than the split maxima for 24·4 at.% Pt, the intensities become about the same for 29·8 at.% Pt and, then, the former become stronger than the latter for 35·0 at.% Pt.

By the use of an electron-microscope hot stage, it was also confirmed in the present case that quenched specimens keep the short-range-ordered structures at temperatures above T_c.

For platinum-rich alloys containing 70 and 75·8 at.% Pt, the features of the diffuse scattering are different from those in copper-rich alloys; diffuse maxima with no splitting are seen at 100, 110 and equivalent positions, in addition to relatively strong diffuse maxima at $\frac{111}{222}$ and equivalent positions [see Fig. 7 (*a*) and (*b*)].

4. Discussion

In the approximation of Clapp & Moss (Clapp & Moss, 1966, 1968; Moss & Clapp, 1968), the intensity of the diffusely scattered X-rays (or electrons or neutrons) at $T > T_c$ is given by

$$I(\mathbf{k}) = C\left\{1 - \frac{T_c}{T}\frac{V(\mathbf{k})}{V(\mathbf{k}_m)}\right\}^{-1}, \qquad (1)$$

where $V(\mathbf{k})$ is a Fourier transform of the pair interaction, $V(\mathbf{r}) = \frac{1}{2}\{V^{AA}(\mathbf{r}) + V^{BB}(\mathbf{r}) - 2V^{AB}(\mathbf{r})\}$, between pairs of atoms separated by the vector $\mathbf{r}$. $V(\mathbf{k}_m)$ is the minimum value of $V(\mathbf{k})$ which occurs at the position $\mathbf{k}_m$, and C is a normalization constant. Through this equation, the diffuse scattering reflects the shape of $V(\mathbf{k})$.

In metallic solid solutions, the conduction electrons have an important contribution to the pair-interaction energy. In the second approximation of the perturbation theory, the effective pair interaction due to the conduction electrons should have characteristic features of a similar nature to the Kohn anomalies which are known in phonon scattering, and a characteristic singularity of $V(\mathbf{k})$ should occur at $\mathbf{k} = 2\mathbf{k}_F$, where $\mathbf{k}_F$ is the Fermi wave vector (Krivoglaz, 1969). The form of the singularity depends on the curvature of the Fermi surface. A spherical surface gives a logarithmic singularity in the derivative of $V(\mathbf{k})$ at $\mathbf{k} = 2\mathbf{k}_F$, but this singularity affects $I(\mathbf{k})$ only a little. For flat areas of the Fermi surface, however, there is a logarithmic singularity in $V(\mathbf{k})$ itself at $2\mathbf{k}_F$, where a pronounced minimum in $V(\mathbf{k})$ may appear, and according to equation (1) a maximum in the diffuse-scattering intensity may correspondingly appear in the reciprocal space. This is the Fermi-surface-imaging idea proposed by Krivoglaz (1969).

If the parts of the Fermi surface normal to, *e.g.* the

Table 2. *Values of separation m measured in terms of the distance between* 000 *and* 200 *spots for* Cu–Pt *alloys*

Composition x in $Cu_{1-x}Pt_x$	Quenching temperature (°C)	m measured at quenched state	m measured at 550 °C
0·244	680	0·085 ± 0·005	
0·270	560	0·100 ± 0·005	
0·298	540	0·114 ± 0·005	0·11 ± 0·1
0·350	700	0·153 ± 0·005	
0·392	760	0·184 ± 0·008	
0·446	900	0·232 ± 0·008	

⟨110⟩ directions are flat, four diffuse maxima will be observed at the intersections of diffuse-intensity regions at a distance of $2\mathbf{k}_F$ from the reciprocal-lattice points, as illustrated in Fig. 8. Moss (1969) explained the split diffuse maxima observed from disordered Cu–Au alloys in this way.

If the short-range-order diffuse scattering depends on the form of the Fermi surface, it must change with the number of conduction electrons in the alloy, since k_F is related to the electron–atom ratio, e/a. If the whole shape of the Fermi surface is assumed to be approximately spherical, the relation between the separation m defined in Fig. 8 and e/a is given as

$$m=\left(\frac{12}{\pi}\frac{e}{a}\right)^{1/3} t-\sqrt{2}\,, \qquad (2)$$

where t is a truncation factor which gives a measure of the non-sphericity of the Fermi surface and is defined as shown in Fig. 9. Hashimoto & Ogawa (1970) studied the behaviour of the diffuse scattering of disordered Cu_3Au by changing the e/a value by adding Pd or In to the alloy, and showed that the observed e/a dependence of m is explained well by equation (2) with $t=$ 0·95. The composition dependence of the diffuse-scattering distribution from disordered copper-rich Cu–Al alloys has also been interpreted similarly by Schattergood, Moss & Bever (1970).

The result in the present experiment that the separation m between split diffuse maxima in the Cu–Pd and Cu–Pt systems changes with Pd or Pt content strongly suggests that the pair-interaction potential in these alloys mainly originates from conduction electrons and that the diffuse scattering reflects the form of the Fermi surface, *i.e.* the diffuse split maxima reflect the flatness of the Fermi surface normal to the ⟨110⟩ directions, as observed in disordered Cu–Au and copper-rich Cu–Al alloys. Fig. 10 shows the measured values of m plotted against composition. The e/a values given in this Figure were calculated from the composition, assuming the number of conduction electrons to be zero for Pd and Pt and one for Cu. It is seen that $m=0$ when $e/a\simeq 0{\cdot}87$, and the absolute value of m increases with decreasing e/a. This behaviour is explained well by equation (2). The three curves in Fig. 10 are those corresponding to $t=0{\cdot}95$, 0·93 and 0·91. The negative values of m in the range of e/a smaller than about 0·87 correspond to the case in which the magnitude of $\mathbf{k}_F$ is smaller than half the distance between 000 and 110. In this case the loci of the points at the distance $2\mathbf{k}_F$ from the reciprocal-lattice points form streaks of the shape shown in Fig. 11, in the reciprocal-lattice plane including $hk0$ reflexions. On the other hand the streaks shown in Fig. 8 are those corresponding to e/a values larger than 0·87 for which m is positive. The diffuse streaks of the former type (Fig. 11) were actually observed in the patterns with [001] incidence, as already described in the preceding section.

The Fermi-surface-imaging theory can similarly be applied to other reciprocal-lattice points. Around the 100 position, for example, four diffuse-intensity regions are expected at a distance $2\mathbf{k}_F$ from the reciprocal-lattice points, 111, $\bar{1}11$, $11\bar{1}$ and $\bar{1}1\bar{1}$, and hence, four diffuse maxima at the intersections of these regions. The twofold splitting observed at the 100 positions in the diffraction patterns with [001] incidence [Fig. 1(*a*)–(*e*) and Fig. 5 (*a*), (*b*)] is interpreted in this way. It should be noted that this twofold splitting is considerably elongated parallel to the vector from 000 to 100. This means that the diffuse-intensity regions at the distance $2\mathbf{k}_F$ consist of slightly curved surfaces, reflecting the flat areas of the Fermi surface. Most of the diffuse intensities observed at other orientations, including those about the 001 and 110 positions in the patterns with [1$\bar{1}$0] incidence [Fig. 4 (*a*) and Fig. 6(*a*)–(*c*)], are explained similarly.

It has been suggested that the observation of the short-range-order diffuse scattering from disordered alloys will be useful in determining the shape of the Fermi surface when it is not theoretically known with precision or when other methods are not effective (Hashimoto & Ogawa, 1970; Castles, Cowley & Spargo, 1971). Although no theoretical or experimental determination of the Fermi surfaces of disordered Cu–Pd and Cu–Pt alloys has so far been made, it can be concluded from the present experimental results that the Fermi surfaces of copper-rich alloys of both systems have flat regions normal to the ⟨110⟩ directions resembling the form of the Fermi surface of Cu.

It is to be noted that both alloy systems have the periodic one-dimensional or two-dimensional antiphase domain structure in the ordered state, depending on composition and temperature. It has been shown by Sato & Toth (1961, 1962) that, in the stabilization

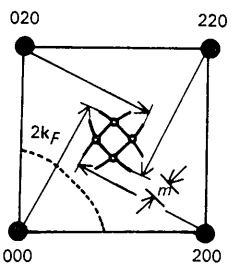

Fig. 8. Illustration of diffuse scattering at the 110 position in the reciprocal space predicted by Moss (1969). The dotted line is a section of the Fermi surface cut by the reciprocal lattice plane including $hk0$ reflexions.

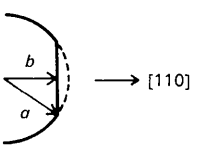

Fig. 9. Definition of the truncation factor, $t=b/a$. The full curve indicates the truncated Fermi surface.

of a long-period anti-phase domain structure, reduction of the energy of the conduction electrons due to the contact of the Fermi surface with Brillouin-zone boundaries plays an important role. From an energy calculation for the conduction electrons, Tachiki & Teramoto (1966) have emphasized that the flatness of the Fermi surface near the ⟨110⟩ directions is most important for the stabilization of the long-period structures. The truncation factor t has been estimated for the ordered Cu–Pd and Cu–Pt alloys, by analysing the available experimental anti-phase-domain size *vs.* composition relations. The value of t estimated in this way is 0·941 for Cu–Pd (Sato & Toth, 1962) and 0·961 for Cu–Pt system (Ogawa *et al.*, 1973). The present analysis, on the other hand, indicates that the values of t for disordered alloys of Cu_3Pd and Cu_3Pt phase regions are in the range of 0·94–0·93, as seen in Fig. 10, and are slightly smaller than those obtained for ordered alloys. It is particularly interesting that for the alloys with Pd or Pt more than 30 at.%, which do not have a long-period structure in the ordered state, there is still the correlation of diffuse-scattering intensity with the flat areas of the Fermi surface, the values of t being in the range of 0·93–0·91 depending on composition. This suggests that the energy of the conduction electrons is still responsible for the pair-interaction potential in these alloys.

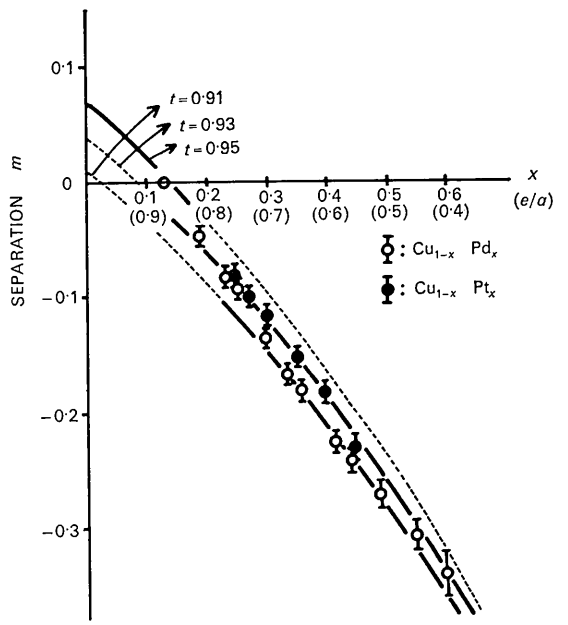

Fig. 10. Measured values of separation m *vs.* composition (electron–atom ratio, e/a). Three curves show the theoretical relation for $t=0{\cdot}95$, 0·93 and 0·91.

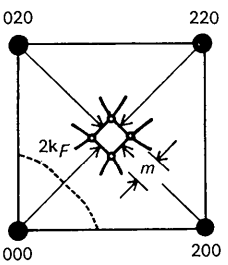

Fig. 11. Illustration of diffuse scattering at the 110 position for the case of $e/a<0{\cdot}87$.

It should be pointed out finally that both alloy systems give additional diffuse-scattering intensities besides those discussed above. For example, diffuse intensities are seen around $\bar{\frac{1}{2}}\frac{3}{2}\bar{\frac{1}{2}}$ and equivalent positions for Cu–Pd alloys irrespective of composition, as indicated by the arrow in Fig. 4 (*b*). It seems that the origin of these intensities and also of the diffuse maxima observed at $\frac{1}{2}\frac{1}{2}\frac{1}{2}$ and equivalent positions for Cu–Pt alloys cannot be attributed to the Fermi-surface effect.* It seems also that diffuse scattering from platinum-rich alloys (70 and 75·8 at.% Pt) has no correlation with the Fermi surface. In order to clarify the nature of these additional diffuse intensities observed in the disordered alloys studied in the present work, it would be necessary to derive $V(\mathbf{k})$ by performing quantitative intensity measurements of diffuse scattering, so that the pair-interaction energies may be obtained.

This work was partly supported by the Grant-in-Aid for Fundamental Scientific Research from the Ministry of Education.

References

BATTERMAN, B. W. (1957). *J. Appl. Phys.* **28**, 556–561.
CASTLES, J. R., COWLEY, J. M. & SPARGO, A. E. C. (1971). *Acta Cryst.* A**27**, 376–383.
CLAPP, P. C. & MOSS, S. C. (1966). *Phys. Rev.* **142**, 418–427.
CLAPP, P. C. & MOSS, S. C. (1968). *Phys. Rev.* **171**, 754–763.
COWLEY, J. M. (1950). *J. Appl. Phys.* **21**, 24–30.
HANSEN, M. & ANDERKO, K. (1958). *Constitution of Binary Alloys*, 2nd ed. New York: McGraw-Hill.
HASHIMOTO, S. & OGAWA, S. (1970). *J. Phys. Soc. Japan*, **29**, 710–721.
HIRABAYASHI, M. & OGAWA, S. (1957). *J. Phys. Soc. Japan*, **12**, 259–271.
JOHANSSON, C. H. & LINDE, I. O. (1927). *Ann. Phys.* **82**, 449–478.
KAPLOW, R. (1958). See S. C. MOSS & P. C. CLAPP (1968), *Phys. Rev.* **171**, 770.
KRIVOGLAZ, M. A. (1969). *Theory of X-ray and Thermal Neutron Scattering by Real Crystals*, New York: Plenum Press.
MARCINKOWSKI, M. J. & ZWELL, L. (1963). *Acta Met.* **11**, 373–390.
MICHIKAMI, O., IWASAKI, H. & OGAWA, S. (1971). *J. Phys. Soc. Japan*, **31**, 956.
MIIDA, R. & WATANABE, D. (1973). *J. Appl. Cryst.* To be published.

* It should be mentioned that there is no correlation between the $\frac{1}{2}\frac{1}{2}\frac{1}{2}$ positions and the superlattice-reflexion positions for the ordered structures, Cu_3Pd (α' and α'') and Cu_3Pt, whereas the sharp spots from the ordered CuPt structure appear at these positions.

MOSS, S. C. (1966). *Local Atomic Arrangements Studied by X-ray Diffraction.* Edited by J. B. COHEN and J. E. HILLIARD. pp. 95–122. New York: Gordon and Breach.
MOSS, S. C. (1969). *Phys. Rev. Lett.* **22**, 1108–1111.
MOSS, S. C. & CLAPP, P. C. (1968). *Phys. Rev.* **171**, 764–777.
OGAWA, S., IWASAKI, H. & TERADA, A. (1973). *J. Phys. Soc. Japan.* **34**, 384–390.
PEARSON, W. B. (1958). *A Handbook of Lattice Spacings and Structures of Metals and Alloys.* Oxford: Pergamon Press.
RAETHER, H. (1952). *Angew. Phys.* **4**, 53–59.
ROBERTS, B. W. (1954). *Acta Met.* **2**, 597–603.
SATO, H. & TOTH, R. S. (1961). *Phys. Rev.* **124**, 1833–1847.
SATO, H. & TOTH, R. S. (1962). *Phys. Rev.* **127**, 469–484.
SATO, K., WATANABE, D. & OGAWA, S. (1962). *J. Phys. Soc. Japan*, **17**, 1647–1651.
SCATTERGOOD, R. O., MOSS, S. C. & BEVER, M. B. (1970). *Acta Met.* **18**, 1087–1098.
SCHNEIDER, A. & ESCH, U. (1944). *Z. Elektrochem.* **50**, 290–301.
SCHUBERT, K., KIEFER, B., WILKENS, M. & HAUFLER, R. (1955). *Z. Metallk.* **46**, 692–715.
TACHIKI, M. & TERAMOTO, K. (1966). *J. Phys. Chem. Solids*, **27**, 335–348.
WALKER, C. B. (1952). *J. Appl. Phys.* **23**, 118–123.
WATANABE, D. (1959). *J. Phys. Soc. Japan*, **14**, 436–443.
WATANABE, D. & FISHER, P. M. J. (1965). *J. Phys. Soc. Japan*, **20**, 2170–2179.
WATANABE, D. & OGAWA, S. (1956). *J. Phys. Soc. Japan*, **11**, 226–239.
WILKINS, S. (1970). *Phys. Rev.* B**2**, 3935–3942.

Acta Cryst. (1973). A**29**, 526

On the Use of in-Pile Collimators in Inelastic Neutron Scattering

BY J. KALUS

Physik-Department der Technischen Universität München, 8000 *München, Arcisstrasse* 21, *Germany (BRD)*

AND B. DORNER*

Institut Max von Laue–Paul Langevin, B.P. 156, 38042-*Grenoble Cedex, France*

(*Received* 16 *January* 1973; *accepted* 28 *March* 1973)

The influence of an in-pile collimator is shown for two cases: *A*. Divergence α_0 of the incoming beam large compared to the mosaic width η of the monochromating crystal and the divergence α_1 after the crystal ($\alpha_0 > \eta, \alpha_1$). *B*. $2\eta > \alpha_0, \alpha_1$. If the same energy resolution for a three-axis spectrometer is required, an optimized comparison of the counting rates in these two cases reveals a factor of *two* in favour of case *B*. This is an important reduction in measuring time for investigations of horizontal dispersion branches, for quasielastic and incoherent scattering, where only the energy (no momentum) resolution is concerned.

1. Introduction

The impression that an in-pile collimator is useless was gained in many discussions the authors have had with scientists performing inelastic neutron-scattering experiments. Therefore we looked into this problem in more detail and found that it is indeed very useful in many cases.

For inelastic neutron-scattering experiments performed with a three-axis spectrometer one uses Bragg reflexion for the monochromation and analysis of the neutrons.

The Bragg law is

$$k = \frac{\pi}{d \cdot \sin \theta_B} \qquad (1)$$

where k is the wave number of the Bragg scattered neutrons, θ_B the Bragg angle and d the spacing of the reflecting lattice planes.

The distribution of the Bragg-reflected neutrons, characterized by the distribution of wave vectors **k**, depends on the collimations α_0 and α_1 before and after reflexion and on the mosaic width η in the crystal. This holds for the monochromator as well as for the analyser.

In the following sections we discuss the cases $\alpha_0 > \eta, \alpha_1$ and $2\eta > \alpha_0, \alpha_1$. For these two cases the shape of the **k** distribution of the reflected neutrons changes appreciably. In § 4 we show that the counting rate of a three-axis spectrometer is different for these two cases. Given a certain overall energy resolution of the apparatus we make an optimization by looking for the best set of the parameters α_0, α_1 and η for the two cases.

2. Case *A*. Neutron monochromation for $\alpha_0 > \eta, \alpha_1$

The hatched region in Fig. 1 shows the momentum distribution of the Bragg-scattered neutrons having a collimator for the incoming neutrons only, characterized by the collimation angle α_0. The distribution of the **k** vectors, taken across the incoming white neutron beam, is indicated by the dotted area. The effect of a second collimator for the scattered neutrons, characterized by the collimation angle α_1 is shown by cross hatching in the reflected beam only.

* On leave from Institut für Festkörperforschung, KFA-Jülich, Germany (BRD).